Coupled operational optimization of smart valve system subject to different approach angles of a pipe contraction

Peiman Naseradinmousavi, Sahar Ghanipoor Machiani, Mohammad A. Ayoubi & C. Nataraj

Structural and Multidisciplinary Optimization

ISSN 1615-147X
Volume 55
Number 3

Struct Multidisc Optim (2017)
55:1001-1015
DOI 10.1007/s00158-016-1554-7

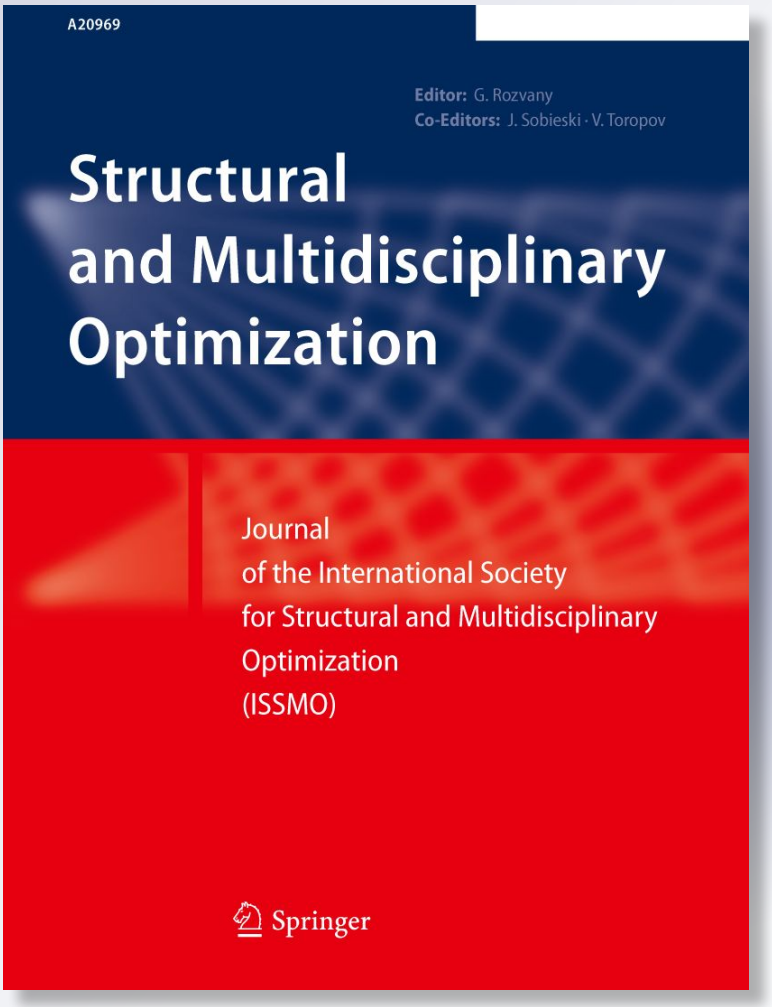

Springer

Struct Multidisc Optim (2017) 55:1001–1015
DOI 10.1007/s00158-016-1554-7

RESEARCH PAPER

Coupled operational optimization of smart valve system subject to different approach angles of a pipe contraction

Peiman Naseradinmousavi[1] · Sahar Ghanipoor Machiani[2] · Mohammad A. Ayoubi[3] · C. Nataraj[4]

Received: 7 April 2016 / Revised: 24 July 2016 / Accepted: 28 July 2016 / Published online: 12 August 2016

Abstract In this paper, we focus on interconnected trajectory optimization of two sets of solenoid actuated butterfly valves dynamically coupled in series. The system undergoes different approach angles of a pipe contraction as a typical profile of the so-called "Smart Valves" network containing tens of actuated valves. A high fidelity interconnected mathematical modeling process is derived to reveal the expected complexity of such a multiphysics system dealing with electromagnetics, fluid mechanics, and nonlinear dynamic effects. A coupled operational optimization scheme is formulated in order to seek the most efficient trajectories of the interconnected valves minimizing the energy consumed enforcing stability and physical constraints. We examine various global optimization methods including Particle Swarm, Simulated Annealing, Genetic, and Gradient based algorithms to avoid being trapped in several possible local minima. The effect of the approach angles of the pipeline contraction on the amount of energy saved is discussed in detail. The results indicate that a substantial amount of energy can be saved by an intelligent operation that uses flow torques to augment the closing efforts.

Keywords Coupled operational optimization · Smart actuated valve · Interconnected modeling · Pipe contraction

✉ Peiman Naseradinmousavi
pnaseradinmousavi@mail.sdsu.edu

Sahar Ghanipoor Machiani
sghanipoor@mail.sdsu.edu

Mohammad A. Ayoubi
maayoubi@scu.edu

C. Nataraj
nataraj@villanova.edu

[1] Dynamic Systems and Control Laboratory, Department of Mechanical Engineering, San Diego State University, San Diego, CA 92115, USA

[2] Department of Civil, Construction, and Environmental Engineering, San Diego State University, San Diego, CA 92115, USA

[3] Department of Mechanical Engineering, Santa Clara University, Santa Clara, CA, 95053, USA

[4] The Villanova Center for Analytics of Dynamic Systems (VCADS), Villanova University, Villanova, PA 19085, USA

1 Introduction

Optimization of multi-agent and large-scale electromechanical systems has received much attention due to the potential to reduce energy consumption considerably leading to savings of significant operational and maintenance costs. One of those networks is the flow distribution system being widely used in different applications including municipal piping systems, oil and gas fields, petrochemical plants, and the US Navy chilled water systems (Hughes et al. 2006; Lequesne et al. 1998). The so-called "Smart Valves" network has received considerable attention to be safely designed and then efficiently operated in critical missions. The main objective of the smart valves is to shut down automatically in case of breakage and to reroute the flow as needed. Optimal design (Naseradinmousavi et al. 2016), operation, and control are three main steps of minimizing any system energy consumption with respect to various stability and physical constraints. In this effort, we focus on optimizing the dynamically interconnected valve trajectories in order to reduce the lumped amount of energy consumed in the coupled actuation units.

We have carried out broad analytical and experimental studies from nonlinear modeling to design optimization of both an isolated and interconnected symmetric butterfly valves driven by solenoid actuators (Naseradinmousavi and Nataraj 2011b, 2012, 2013; Naseradinmousavi 2015, Naseradinmousavi et al. 2016). The multidisciplinary couplings, including electromagnetics and fluid mechanics, had to be thoroughly considered in the modeling phase in order to yield an accurate nonlinear model of such a complex system. A third-order nondimensional dynamic model of the single set was derived to be used in nonlinear dynamic analysis (Naseradinmousavi and Nataraj 2012) and optimal design (Naseradinmousavi and Nataraj 2013).

The dynamic analysis yielded crisis and transient chaotic dynamics of a single actuated valve for some critical physical parameters. A comprehensive stability map was also derived and presented as an efficient tool to determine the safe domain of operation which in turn could serve for identifying the lower and upper bounds for the design optimization efforts. The design optimization was then carried out (Naseradinmousavi and Nataraj 2013) to select the optimal actuation unit's parameters coupled with the mechanical and fluid parts in order to significantly reduce the amount of energy consumption (upward of % 40).

Note that the applications addressed earlier contain scores of actuated valves in which a high level of dynamic coupling has been observed in practice. These dynamic couplings among different sets need to be captured through analytical studies. We have developed (Naseradinmousavi 2015) a novel nonlinear model for two sets of solenoid actuated butterfly valves operating in series. The closing/opening valves were modeled as changing resistors and the flow between them as a constant one. A nonlinear coupled model revealed the high dynamic sensitivity of each element of a set, the valve and the actuator, to another one and vice versa. The power spectrum was used in confirming the same frequency response of a neighbor set due to the external periodic noise applied on another set of the valve and actuator.

In further studies, we optimized the design of coupled actuation units of two sets operating in series (Naseradinmousavi et al. 2016) subject to a sudden contraction. The pipe contraction imposed an additional resistance to be modeled and therefore, the coupled dynamic equations derived in Naseradinmousavi (2015) had to be slightly modified (which we represent here for completeness). We discovered an interesting coupling between currents of the actuation units through the interconnected flow loads, including hydrodynamic and bearing torques, which affect the dynamics of both the valves.

Optimization of electromechanical and multidisciplinary systems has recently received much attention. Klimovich (1997) obtained some optimal decisions for one-and two-dimensional axisymmetrical flow models. Sefkat (2009) has minimized volume and power dissipation by deriving expressions for consumed power, magnetic attraction force, coil temperature and magnet volume, depending on the dimensions. Elka and Bucher (2009) discussed the optimal shape design of segmented spatial sensors and actuators that isolate selected mode shapes and perform modal filtering. Raulli and Maute (2005) addressed the design of electrostatically actuated microelectromechanical systems by topology optimization such that the layout of the structure and the electrode are simultaneously optimized. Grierson and Pak (1993) investigated an approximate design fitness evaluation technique with the aim of improving the numerical efficiency of the genetic search algorithm. Other contributions in operational and design optimization of electromechanical systems include (Lee et al. 1988; Mezyk 1994; Kajima 1995; Messine et al. 1998; Kelley 1999; Sung et al. 2002; Karr and Scott 2003; Baek-Ju and Eun-Woong 2005; Yu et al. 2007; Nowak 2010; Chakraborty et al. 2013; Mahdi 2014).

In this paper, the optimal operation process is formulated to help select the appropriate trajectories of the valves coupled with the electromagnetical, mechanical, and fluid parts in order to yield an energy efficient system. The contribution of this work is to optimize both the valves' trajectories dynamically coupled in different aspects while our previous efforts (Naseradinmousavi and Nataraj 2013, 2015; Naseradinmousavi et al. 2016) were on optimizing the design of the single (by neglecting its dynamic coupling with another set) and coupled actuation units. In this effort, a lumped cost function will be minimized, while enforcing the stability and physical constraints, using four global optimization tools to avoid being trapped in possible local minima along with the objective of obtaining the most efficient operations of the coupled valves.

2 Mathematical modeling

Shown in Fig. 1a is a pair of symmetric butterfly valves driven by solenoid actuators through rack and pinion arrangements. The rack and pinion mechanism provides a kinematic constraint which connects the dynamics of the valve and actuator. Applying DC voltages, as being used in the Navy ships for chilled water systems, the motive forces give translational motions to the actuators' moving parts (plungers) and subsequently the valves rotate to desirable angles. Note that a return spring has been a common practice among industries to open the valves.

Interconnected modeling of such a multiphysics system undoubtedly needs some simplifying assumptions to reduce

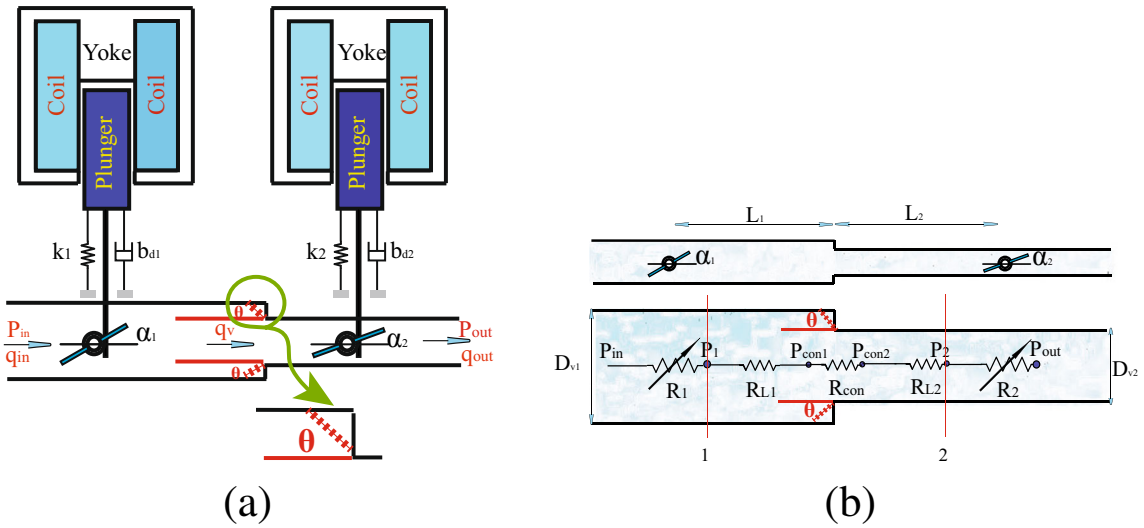

Fig. 1 **a** A schematic configuration of two solenoid actuated butterfly valves subject to the sudden contraction; **b** A coupled model of two butterfly valves in series without actuation

time consuming numerical calculations. The force resulting from the magnetic field need an extremely short period of time to reach its maximum value. This period is the so-called "Diffusion Time" and has an inverse relationship with the amount of current used. Note that using the current of 24 (A) would yield a negligible diffusion time of $\tau_d \approx 2(ms)$ (Naseradinmousavi and Nataraj 2011b) with respect to the nominal operation time of 180(s).

As is commonly done for valve studies, we will assume dominant laminar flow for both the coupled valves to avoid the numerical difficulties involved with a turbulent regime. Note that developing an analytical model is necessary to carry out the dynamic analysis and optimization. Nevertheless, a crucial question needs to be carefully answered with respect to the validity of such an assumption. Using the values of pipe diameter and flow mean velocity listed in Table 1, one can easily distinguish the existence of the turbulent regime which invalidates the assumption we have made. From another aspect, the analytical formulas derived for the flow loads, including the hydrodynamic and bearing torques, have been developed based on the assumption of laminar flow (Park and Chung 2006; Leutwyler and Dalton 2008). To address the issues discussed above, we have carried out experimental work to measure the sum of the hydrodynamic and bearing torques as the most affecting loads on the valves and subsequently, the dynamics of the actuators (Naseradinmousavi et al. 2016). The experiment yielded the total torque for the inlet velocity of $v \approx 2.7\left(\frac{m}{s}\right)$ and valve diameter of $D_v = 2\ (inches)$ reasonably validating the laminar flow assumption (Naseradinmousavi 2012).

The flow torques have been shown to play a highly important role for the dynamics of an isolated solenoid actuated butterfly valve and we hence expect to observe such effects for the interconnected sets (Naseradinmousavi 2015) as well. The coupled system is modeled as a set of five resistors. Two changing resistors represent the closing/opening valves, two constant ones indicate head losses between the valves, and fifth is due to the pipe contraction as shown in Fig. 1b. The inlet and outlet pressures are as shown in Table 1. Using the assumption of the dominant laminar flow, the pressure drops between two valves can be expressed based on the Hagen-Poiseuille (Bennett and Myers 1962) and Borda-Carnot (Massey and Ward-Smith 1998) formulas (points 1 and 2):

$$P_1 - P_{con1} = \underbrace{\frac{128\mu_f L_1}{\pi D_{v1}^4}}_{R_{L1}} q_v \tag{1}$$

$$P_{con1} - P_{con2} = \frac{1}{2} K_{con} \rho v_{out}^2 \tag{2}$$

$$P_{con2} - P_2 = \underbrace{\frac{128\mu_f L_2}{\pi D_{v2}^4}}_{R_{L2}} q_v \tag{3}$$

where, q_v is the volumetric flow rate, μ_f indicates the fluid dynamic viscosity, D_{v1} and D_{v2} are the valves' diameters, L_1 and L_2 stand for the pipe lengths before and after contraction, R_{L1} and R_{L2} indicate the constant resistances, and

Table 1 The system parameters

ρ	$1000\frac{kg}{m^3}$	v	$3\frac{m}{s}$
μ	0.5	P_{in}	256(kPa)
$J_{1,2}$	$0.104 \times 10^{-1}(kg.m^2)$	$b_{d1,d2}$	$8420\frac{N.m.s}{rad}$
N_1	3300	$C_{11,22}$	$1.56 \times 10^6(H^{-1})$
$g_{m1,m2}$	0.1(m)	$V_{1,2}$	24(Volt)
D_{v1}	0.2032(m)	D_{v2}	0.127(m)
$D_{s1,s2}$	0.01(m)	P_{out}	2(kPa)
$k_{1,2}$	$60(N.m^{-1})$	$C_{21,22}$	$6.32 \times 10^8(H^{-1})$
L_1	2(m)	L_2	1(m)
μ_f	$0.018\ (Kg.m^{-1}.s^{-1})$	$R_{1,2}$	$1(\Omega)$
$r_{1,2}$	0.05(m)	θ	90°
N_2	3300		

P_{con1} and P_{con2} are the flow pressures before and after contraction. K_{con} is calculated as the following:

$$K_{con} = 0.5(1-\beta^2)\sqrt{\sin\left(\frac{\theta}{2}\right)} \tag{4}$$

where, β indicates the ratio of minor and major diameters $\left(\frac{D_{v2}}{D_{v1}}\right)$ and θ is the angle of approach shown in Fig. 1a and b. The values listed in Table 1 easily yield $K_{con} = 0.2562$. We then rewrite (2) as follows:

$$\begin{aligned} P_{con1} - P_{con2} &= \frac{1}{2}K_{con}\rho v_{out}^2 \\ &= \underbrace{\frac{8K_{con}}{\pi^2 D_{v2}^4}\rho}_{R_{con}} \underbrace{\frac{\pi^2 D_{v2}^4 v_{out}^2}{16}}_{q_v^2} \\ &= R_{con}q_v^2 \end{aligned} \tag{5}$$

where, R_{con} is the resistance due to the pipe contraction. The pressure drop between the valves can be derived by adding (1), (2), (3) and (5):

$$P_1 - P_2 = [R_{L1} + R_{L2} + R_{con}q_v]q_v \tag{6}$$

The interconnected P_1 and P_2 terms are derived (we have reported in Naseradinmousavi et al. 2016) as follows:

$$P_1 = \frac{R_{n2}P_{in} + R_{n1}P_{out} + R_{n1}(R_{L1} + R_{L2} + R_{con}q_v)q_v}{(R_{n1} + R_{n2})} \tag{7}$$

$$P_2 = \frac{R_{n2}P_{in} + R_{n1}P_{out} - R_{n2}(R_{L1} + R_{L2} + R_{con}q_v)q_v}{(R_{n1} + R_{n2})} \tag{8}$$

where,

$$R_{n1}(\alpha_1) = \frac{e_1}{(p_1\alpha_1^3 + q_1\alpha_1^2 + o_1\alpha_1 + s_1)^2} \tag{9}$$

$$R_{n2}(\alpha_2) = \frac{e_2}{(p_2\alpha_2^3 + q_2\alpha_2^2 + o_2\alpha_2 + s_2)^2} \tag{10}$$

The numerical values of $e_1, p_1, q_1, o_1, s_1, e_2, p_2, q_2, o_2$, and s_2 were reported in Naseradinmousavi et al. (2016). The dynamic sensitivities of P_1 and P_2 to R_{n1}, R_{n2}, R_{L1}, R_{L2}, and R_{con} are distinguishable through (7) and (8). Any slight dynamic changes of the upstream set of the valve-actuator would be expected to be observed for the downstream one, in fact, as often observed in practice. The dependencies of the hydrodynamic and bearing torques on all the resistances are reformulated as follows, which we have reported in Naseradinmousavi et al. (2016).

$$T_{hi} = f_i(\alpha_i)D_{vi}^3\Delta P_i(R_{n1}, R_{n2}, R_{L1}, R_{L2}, R_{con}) \tag{11}$$

$$T_{bi} = C_i\Delta P_i(R_{n1}, R_{n2}, R_{L1}, R_{L2}, R_{con}) \tag{12}$$

f_i is a nonlinear function of the changing T_{ci}, C_{cci}, and the valve rotation angles. To carry out a systematic dynamic analysis, the following functions are fitted to the $D_{vi}^3 f_i$ of each valve (Naseradinmousavi 2012, 2015):

$$\begin{aligned} T_{h1} &= \underbrace{(a_1\alpha_1 e^{b_1{\alpha_1}^{1.1}} - c_1 e^{d_1\alpha_1})}_{D_{v1}^3 f_1}(P_{in} - P_1) \\ &= (a_1\alpha_1 e^{b_1{\alpha_1}^{1.1}} - c_1 e^{d_1\alpha_1}) \times \frac{\frac{e_1}{(p_1\alpha_1^3+q_1\alpha_1^2+o_1\alpha_1+s_1)^2}}{\sum_{i=1}^{2}\frac{e_i}{(p_i\alpha_i^3+q_i\alpha_i^2+o_i\alpha_i+s_i)^2}} \\ &\quad \times (P_{in} - P_{out} - (R_{L1} + R_{L2} + R_{con}q_v)q_v) \end{aligned} \tag{13}$$

$$\begin{aligned} T_{h2} &= \underbrace{(a_1'\alpha_2 e^{b_1'{\alpha_2}^{1.1}} - c_1' e^{d_1'\alpha_2})}_{D_{v2}^3 f_2}(P_2 - P_{out}) \\ &= (a_1'\alpha_2 e^{b_1'{\alpha_2}^{1.1}} - c_1' e^{d_1'\alpha_2}) \times \frac{\frac{e_2}{(p_2\alpha_2^3+q_2\alpha_2^2+o_2\alpha_2+s_2)^2}}{\sum_{i=1}^{2}\frac{e_i}{(p_i\alpha_i^3+q_i\alpha_i^2+o_i\alpha_i+s_i)^2}} \\ &\quad \times (P_{in} - P_{out} - (R_{L1} + R_{L2} + R_{con}q_v)q_v) \end{aligned} \tag{14}$$

The values of $a_1, a_1', b_1, b_1', c_1, c_1', d_1$, and d_1' can be found in Naseradinmousavi et al. (2016).

We have previously derived the rate of current and magnetic force terms (Naseradinmousavi and Nataraj 2011b) which are utilized in developing the sixth-order coupled dynamic model (Naseradinmousavi et al. 2016) as follows.

Note that both the motive force and current are highly sensitive to the plunger displacement and subsequently the valve rotation angle.

$$F_{mi} = \frac{C_{2i} N_i^2 i_i^2}{2(C_{1i} + C_{2i}(g_{mi} - x_i))^2} \tag{15}$$

$$\frac{di_i}{dt} = \frac{(V_i - R_i i_i)(C_{1i} + C_{2i}(g_{mi} - x_i))}{N_i^2} - \frac{C_{2i} i_i \dot{x}_i}{(C_{1i} + C_{2i}(g_{mi} - x_i))} \tag{16}$$

$$\dot{z}_1 = z_2 \tag{17}$$

$$\dot{z}_2 = \frac{1}{J_1}\left[\frac{r_1 C_{21} N_1^2 z_3^2}{2(C_{11} + C_{21}(g_{m1} - r_1 z_1))^2} - b_{d1} z_2 - k_1 z_1 + \frac{\frac{(P_{in} - P_{out} - (R_{L1} + R_{L2} + R_{con} q_v) q_v) e_1}{(p_1 z_1^3 + q_1 z_1^2 + o_1 z_1 + s_1)^2}}{\sum_{i=1,4} \frac{e_i}{(p_i z_i^3 + q_i z_i^2 + o_i z_i + s_i)^2}} \times \left[(a_1 z_1 e^{b_1 {z_1}^{1.1}} - c_1 e^{d_1 z_1}) - C_1 \times \tanh(K z_2)\right]\right] \tag{18}$$

$$\dot{z}_3 = \frac{(V_1 - R_1 z_3)(C_{11} + C_{21}(g_{m1} - r_1 z_1))}{N_1^2} - \frac{r_1 C_{21} z_3 z_2}{(C_{11} + C_{21}(g_{m1} - r_1 z_1))} \tag{19}$$

$$\dot{z}_4 = z_5 \tag{20}$$

$$\dot{z}_5 = \frac{1}{J_2}\left[\frac{r_2 C_{22} N_2^2 z_6^2}{2(C_{12} + C_{22}(g_{m2} - r_2 z_4))^2} - b_{d2} z_5 - k_2 z_4 + \frac{\frac{(P_{in} - P_{out} - (R_{L1} + R_{L2} + R_{con} q_v) q_v) e_2}{(p_2 z_4^3 + q_2 z_4^2 + o_2 z_4 + s_2)^2}}{\sum_{i=1,4} \frac{e_i}{(p_i z_i^3 + q_i z_i^2 + o_i z_i + s_i)^2}} \times \left[(a_1' z_4 e^{b_1' {z_4}^{1.1}} - c_1' e^{d_1' z_4}) - C_2 \times \tanh(K z_5)\right]\right] \tag{21}$$

$$\dot{z}_6 = \frac{(V_2 - R_2 z_6)(C_{12} + C_{22}(g_{m2} - r_2 z_4))}{N_2^2} - \frac{r_2 C_{22} z_5 z_6}{(C_{12} + C_{22}(g_{m2} - r_2 z_4))} \tag{22}$$

where, b_d indicates the equivalent torsional damping, K_t is the equivalent torsional stiffness, V stands for the supply voltage, x is the plunger displacement, r indicates the radius of the pinion, C_1 and C_2 are the reluctances of the magnetic path without air gap and that of the air gap, respectively, F_m is the motive force, N stands for the number of coils, i indicates the applied current, g_m is the nominal airgap, J indicates the polar moment of inertia of the valve's disk, and R is the electrical resistance of coil. $z_1 = \alpha_1$, $z_2 = \dot{\alpha}_1$, and $z_3 = i_1$ indicate the upstream valve's rotation angle, angular velocity, and actuator current, respectively. $z_4 = \alpha_2$, $z_5 = \dot{\alpha}_2$, and $z_6 = i_2$ stand for the downstream valve's rotation angle, angular velocity, and actuator current, respectively.

3 Optimal operation

The stability and physical constraints reported in Naseradinmousavi and Nataraj (2011a, 2012) undoubtedly demand robust optimization schemes to be utilized in minimizing the energy consumed by two coupled sets. Note that operating the system without the constraints determined through the nonlinear dynamic analysis would undesirably lead to the catastrophic failure of the network shown in Fig. 2a revealing the hyperchaotic dynamics of both the actuated valves. It can in fact be shown that some critical values of the equivalent viscous damping and friction coefficient of the bearing area ($\mu_i = b_{di} = 10^{-7}$) yield the hyperchaotic dynamics for the initial values of $\alpha_{10} = \alpha_{20} = 3°$. The hyperchaotic dynamics happens for the systems of order higher than four ($n \geq 4$) and can be recognized by revealing at least two positive Lyapunov

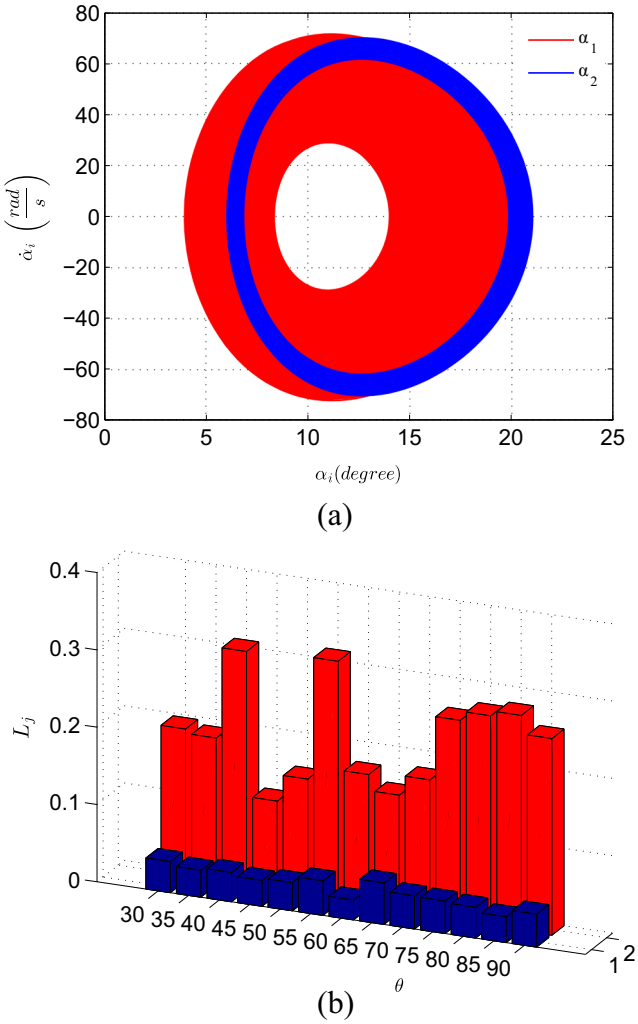

Fig. 2 **a** Chaotic dynamics of the valves/actuators; **b** Two positive Lyapunov exponents spectra vs. the approach angle indicating the hyperchaotic dynamics of the system

exponents. Shown in Fig. 2b reveals two positive Lyapunov exponents not only for the sudden pipe contraction but also for a broad range of the approach angles (θ) indicating the hyperchaotic dynamics of both the coupled valves. The hyperchaotic motions reveal higher stochastic amplitude of oscillations than those of chaotic ones. This would lead us to carry out a constrained optimization effort to avoid being exposed to such dangerous dynamical behaviors.

The problem at hand is a constrained optimization problem with possibly several local minima. Therefore, we have to employ robust optimization algorithms to capture the global minimum. The cost function we wish to minimize is a sum of the energy used in both the sets.

$$\min E_{tot} = \sum_{i=1}^{2} \int_0^{t_f} V i_i \, dt \tag{23}$$

subject to: $z_1 < 90^\circ$, $z_4 < 90^\circ$

& Coupled Dynamic Equations

We then fit two nonlinear curves to the nominal valve trajectories obtained via (17)–(22):

$$\alpha_1(t) = A \tanh(Bt^4) \tag{24}$$

$$\alpha_2(t) = C \tanh(Dt^4) \tag{25}$$

The nominal values of A, B, C, and D are listed in Table 2. The curves fitted to the nominal trajectories are selected based on desirable smooth valve rotations. The so-called "S-Shaped" valves' motions have traditionally been appropriate trajectories to avoid dangerous behaviors such as the well-known water hammering, in particular, for such critical applications addressed earlier. A, B, C, and D are variables that we need to optimize in order to identify the most efficient valve trajectories yielding minimum energy consumption by using the DC voltage sources ($V_1 = V_2 = 24(Volts)$). Note that $\alpha_1(t)$ and $\alpha_2(t)$ are coupled angles through the interconnected dynamic equations. We next collect the coefficients into a vector:

$$\theta_1 = [A, B, C, D]^T \tag{26}$$

The coupled equations, as discussed earlier, need to be satisfied at all times during the optimization process and the coefficients are subject to the following lower and upper bounds.

$$\theta_{1min} = [0.8, 0.1 \times 10^{-7}, 0.92, 0.1 \times 10^{-7}]^T \tag{27}$$

$$\theta_{1max} = [0.85, 9.50 \times 10^{-5}, 0.98, 5.99 \times 10^{-5}]^T \tag{28}$$

These bounds were determined based on practical system considerations, stability analysis (Naseradinmousavi and Nataraj 2012; Naseradinmousavi 2012), and physical constraints. We employ four global optimization tools including simulated annealing, genetic, particle swarm, and gradient based algorithms to provide a clear map of optimization efforts with respect to the locality/globality of the cost function minima.

We have thoroughly reported the advantages of simulated annealing (Kirkpatrick et al. 1983; Cerny 1985), genetic (Holland 1975), and gradient based algorithms in Naseradinmousavi et al. (2016). The particle swarm optimization (PSO) was originally developed by Kennedy, Eberhart and Shi (Kennedy and Eberhart 1995; Shi and Eberhart 1998) and was first used in simulating social behaviour. PSO is metaheuristic as it makes few or no assumptions about the problem being optimized and can search very large spaces of candidate solutions.

We have used Global Search algorithm in Matlab which utilizes gradient-based method to return local and global minima. The algorithm starts a local solver (here fmincon) from multiple starting points and stores local and global solutions found during the search process. The fmincon solver estimates gradients by parallel finite differences. Note that the global search solver uses a scatter-search algorithm to generate multiple starting points which can be observed in figures shown in results section for presenting the gradient-based method. It also runs a constrained nonlinear optimization solver to search for a local minimum from the remaining start points. We have defined function (TolFun) and constraints (TolCon) tolerances of 10^{-12} for all the algorithms. To facilitate the scatter-search algorithm, in particular for the gradient-based and simulated annealing methods, we use random initial guesses as follows:

$$\theta_{1rn} = \theta_{1min} + (\theta_{1max} - \theta_{1min}) \times rand(1)$$

Table 2 The nominal and optimal variables

	Nominal	GB	GA	SA	PS
A	0.83	0.811	0.81	0.81	0.8458
$B \times 10^7$	1	0.29	0.29	0.29	0.29
C	0.95	0.94	0.94	0.94	0.94
$D \times 10^7$	1	0.2921	0.29	0.29	0.29
Energy (J)	206880	177180	176900	176900	176887

where, rand(1) is a random number between zero and one.

Note that the coefficients are not of the same order, and resulted in serious numerical errors. We fixed this problem by conditioning them using a normalization scheme as follows.

$$A_n = A \times 10^3;\ B_n = B \times 10^7$$
$$C_n = C \times 10^3;\ D_n = D \times 10^7$$

Note that for the PS algorithm, we have utilized 1) "MaxIter" of 1200 which indicates maximum number of iterations (300×nvar (nvar here is 4)), 2) "MinFractionNeighbors" of 0.25 which is minimum adaptive neighborhood size, 3) "SelfAdjustment" of 1.49 which stands for weighting of each particle's best position when adjusting velocity, 4) "SocialAdjustment" of 1.49 which indicates weighting of the neighborhood's best position when adjusting velocity, and 5) "SwarmSize" of 100 (min(100, 100× nvar)) for number of particles in the swarm.

For the GA method we have used 1) "PopulationSize" of 50 for the size of population, 2) "Generations" of 1200 which indicates the maximum number of iterations before the algorithm halts, 3) "MigrationFraction" of 0.2 specifying the fraction of individuals in each subpopulation that migrates to a different subpopulation, 4) "MigrationInterval" of 20 standing for the number of generations that take place between migrations of individuals between subpopulations, and 5) Function (TolFun) and constraints (TolCon) tolerances of 10^{-12}.

4 Results

The sensitivity analysis, either local or global, is an efficient tool to investigate the effects of changes of the optimization variables on the cost function defined. Shown in Fig. 3a–d are results of such a local analysis (one-at-a-time (OAT) technique) with respect to the stability bounds which we have determined in Section 3. Note that the OAT method analyzes the effect of one variable on the cost function at a time while keeping the other variables constant. However, the global sensitivity analysis uses set of samples to search the design space.

The gradient of the cost function is numerically calculated with respect to the optimization variables as follows:

$$\nabla E = \left[\frac{\partial E}{\partial A}, \frac{\partial E}{\partial B}, \frac{\partial E}{\partial C}, \frac{\partial E}{\partial D}\right]^T$$

It is of great interest to observe that Fig. 3a–d reveal significant roles of B and D, in particular D of the downstream set, on the considerable changes of the lumped cost function. On the other hand, the optimization process is too sensitive to the variables of B and D than A and C. The physical interpretation of such an interesting situation can be found through the dynamics of flow loads which we will discuss in detail via Fig. 9; the downstream set plays a more significant role in yielding the coupled efficient trajectories. Note that B and D, in particular D, directly affect angular velocities of both the valves which in turn would lead to reduced currents used in both the sets, which we will present and discuss via Figs. 7, 8 and 9. Note that the results of global sensitivity analysis, as shown in Fig. 4a–d, also confirm the highly effective roles of B and D on the optimization process.

Table 1 contains the parameters obtained from the experimental work we carried out for the isolated set (Naseradinmousavi et al. 2016). Figures 5 and 6 reveal the optimization process for the coefficients of curves fitted to the valve angles using the genetic (GA), gradient based (GB), simulated annealing (SA), and particle swarm (PS) algorithms. The GB, GA, SA, and PS algorithms terminate after 13797, 1100, 7685, and 1170 iterations, respectively, satisfying the tolerances defined for both the variables and the lumped cost function. The computational times for the GB, GA, SA, and PS methods are 4860 s, 720 s, 2212 s, and 762 s, respectively. It is of great interest to observe that all methods result in lower values of B, C, and D with respect to their corresponding nominal values listed in Table 2, which in turn would yield slower responses of both the valves than those of the nominal ones. The GB, SA, GA methods lead to lower values of A but the PS yields a slightly higher value in comparison with the nominal one . It is straightforward to conclude that the PS algorithm is more efficient with respect to the computational time while it yields the minimal energy consumption than other methods, as shown in Table 2.

Such optimal motions would lead to considerably lower values of the currents of both the actuation units in comparison with the nominal ones, particularly for the downstream set as shown in Figs. 7 and 8. A sudden current drop is distinguishable for the downstream actuator (Fig. 8) at t = 34(s). The physical interpretation of such lower values of the currents can be found through the flow dynamics (loads) interconnected with the electromagnetic parts. We have previously established (Naseradinmousavi et al. 2016) that the change of pipe diameter would potentially yield higher values of the hydrodynamic torque acting on the downstream valve than that of the upstream one:

$$\frac{T_{h2}}{T_{h1}} \propto \left(\frac{D_{v2}}{D_{v1}}\right)^3 \times \left(\frac{c_{v1}}{c_{v2}}\right)^2 \tag{29}$$

The downstream valve is logically expected, for both the nominal and optimal cases, to be subject to the higher hydrodynamic torque (Naseradinmousavi and Nataraj 2013) as shown in Fig. 9. We have also discussed the highly important role of the hydrodynamic torque on the valves' operations. The hydrodynamic torque acts as a helping load

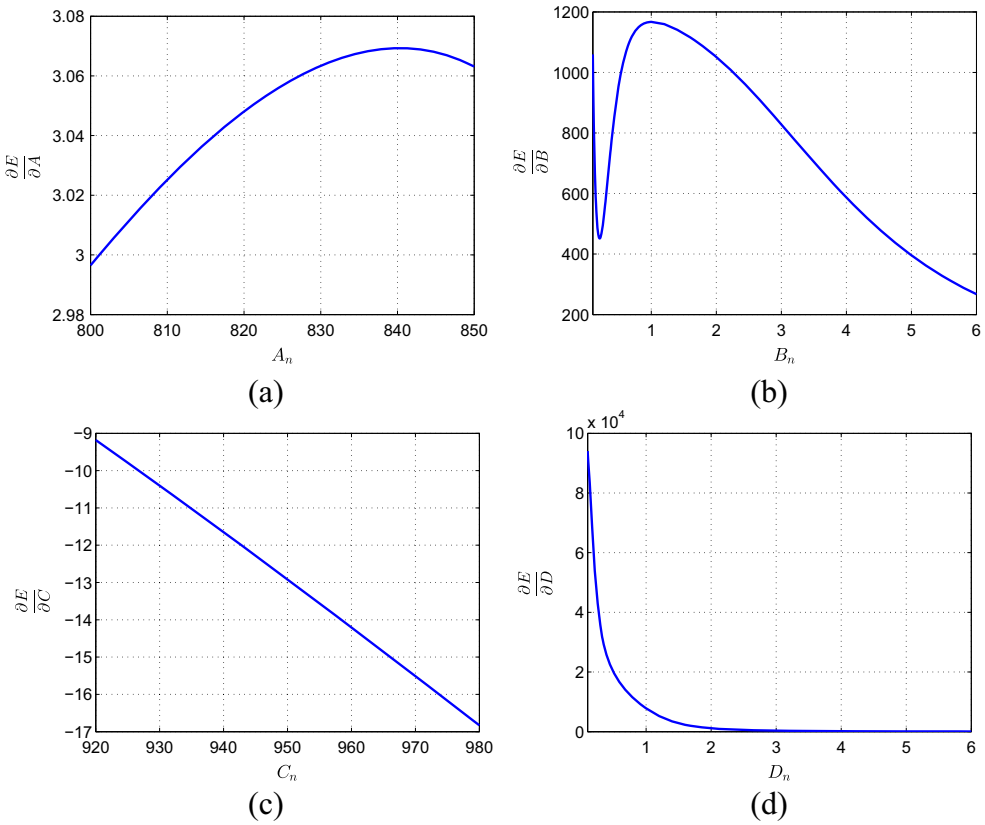

Fig. 3 The local sensitivity analysis; the gradient of the cost function with respect to the optimization variables

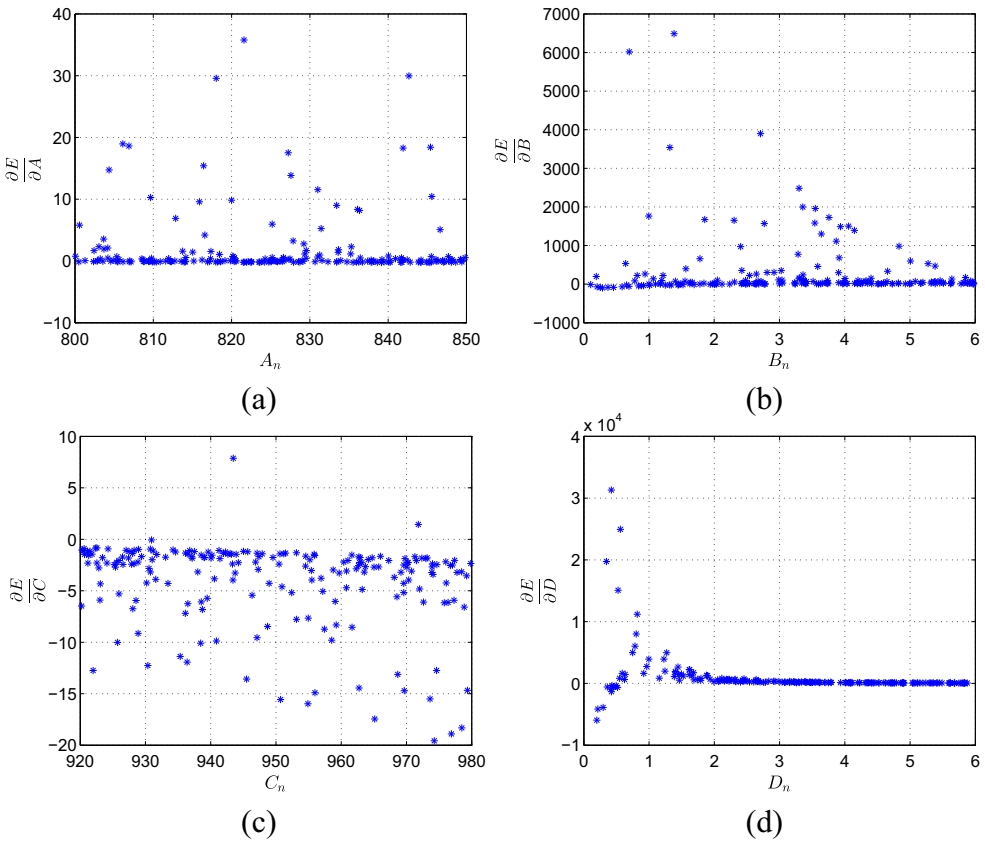

Fig. 4 The global sensitivity analysis; the gradient of the cost function with respect to the optimization variables

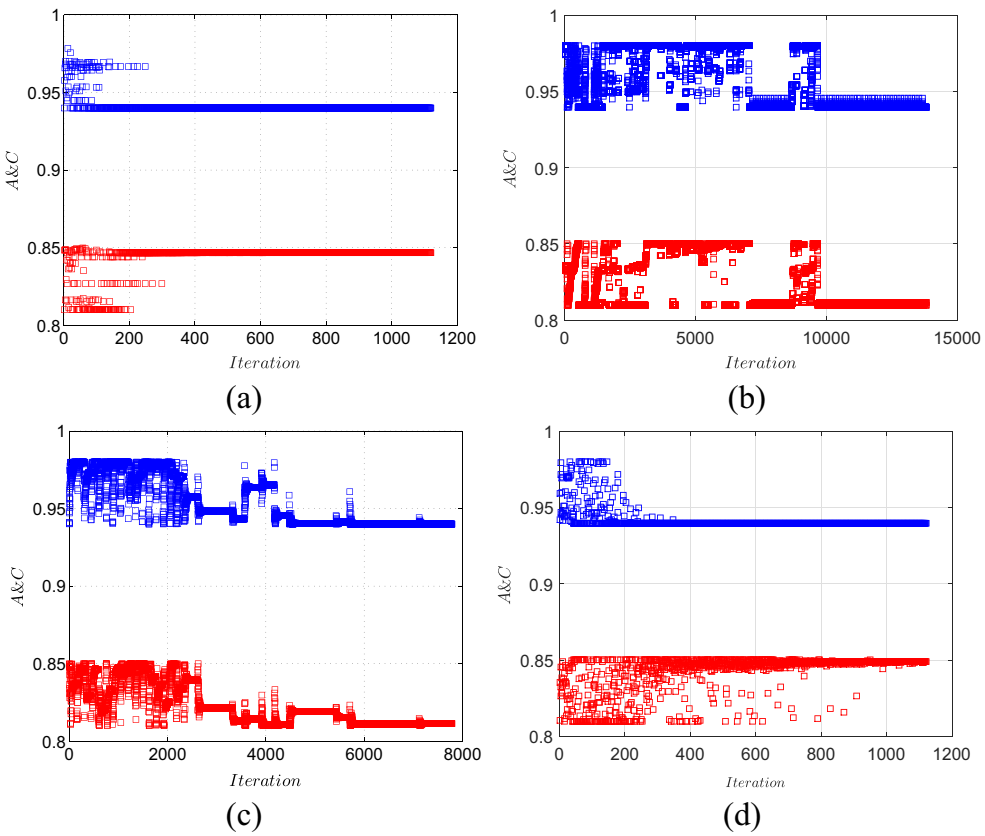

Fig. 5 The optimized A and C: red and blue squares stand for A and C, respectively; **a** GA; **b** GB; **c** SA; **d** PS

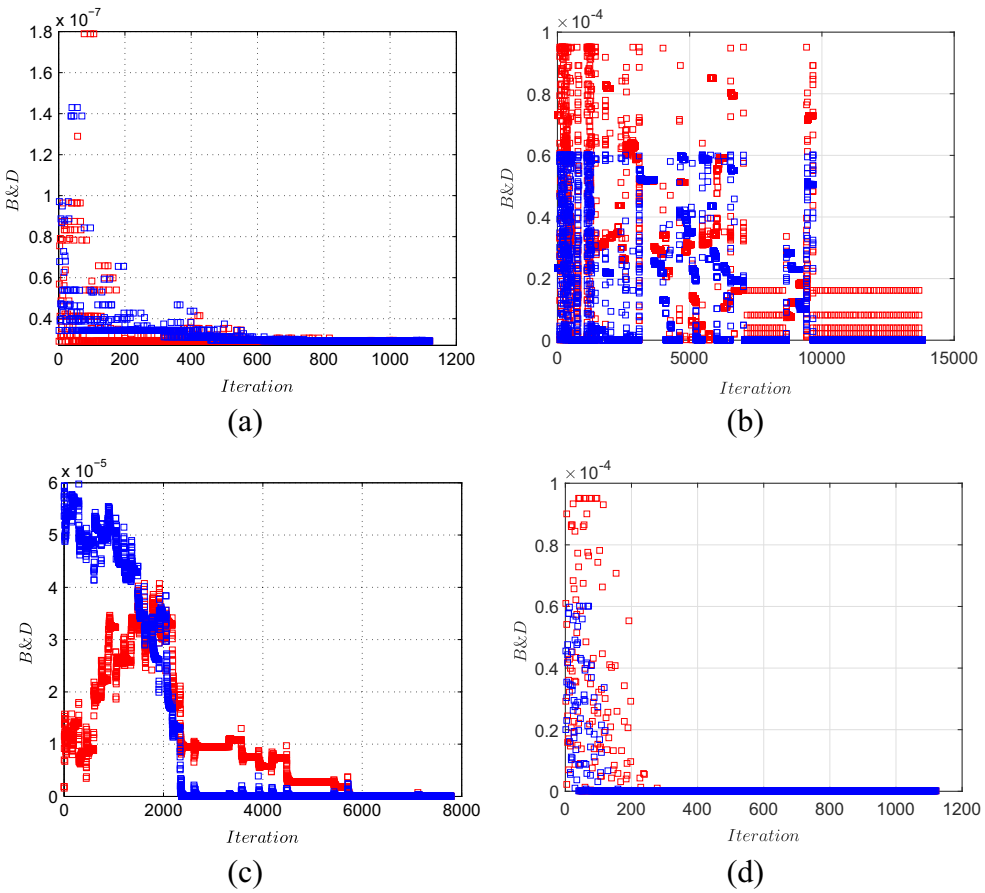

Fig. 6 The optimized B and D: red and blue squares stand for B and D, respectively; **a** GA; **b** GB; **c** SA; **d** PS

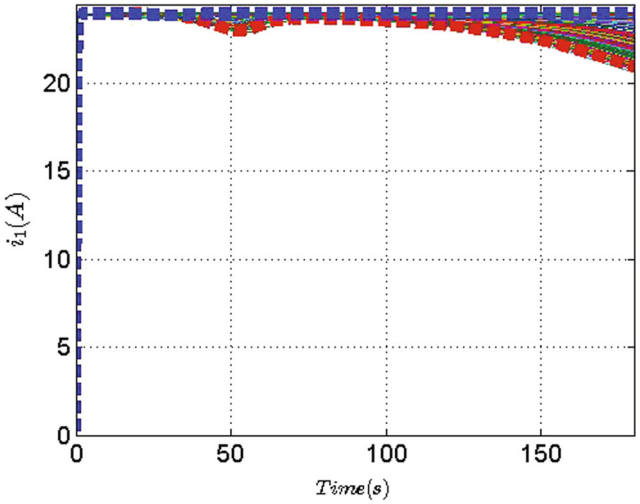

Fig. 7 The optimal (*dashed red line*) and nominal (*dashed blue line*) applied currents of the upstream set

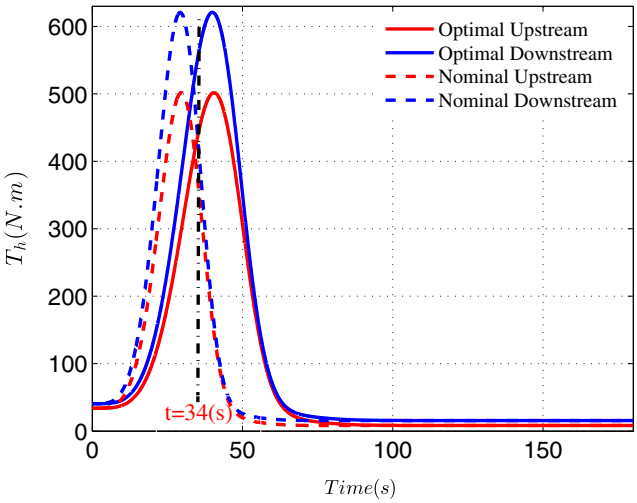

Fig. 9 The hydrodynamic torque acting on both the valves

pushing the valve to be closed and is typically effective for when the valve angle is lower than 60° (Naseradinmousavi 2015; Naseradinmousavi et al. 2016); the effective range was experimentally examined (Naseradinmousavi 2015) confirming the helping behavior of the hydrodynamic torque by presenting positive values. Consequently, the higher helping torques would result in the downstream valve's higher rotation angles than those of the upstream ones (for both the nominal and optimal configurations), as shown in Fig. 10; $\alpha_{1no} = 47°$, $\alpha_{2no} = 52.9°$, $\alpha_{1op} = 48°$, and $\alpha_{2op} = 52.73°$.

Note that Fig. 10 presents the valves' relatively slower motions for the optimal operations in comparison with the nominal ones. These kinds of operationally optimized rotations expose both the coupled valves to the higher hydrodynamic torques (as helping factors) in comparison with the nominal loads, as shown in Fig. 9. This is explicitly distinguishable at t = 34(s) by showing the higher hydrodynamic torques afterward and the actuators have subsequently more freedom to act with significantly lower currents, in particular, for the downstream set as it undergoes the higher hydrodynamic load. The optimal motions would lead us to consume a lower amount of energy as presented in Fig. 11.

The decreased amounts of energies are spent as shown in Fig. 11a, b, c and d. Shown in Fig. 11a, b, c and d indicate 14.3 %, 14.4 %, 14.4 %, and 14.5 % energy savings through the GA, GB, SA, and PS algorithms, respectively. Note that

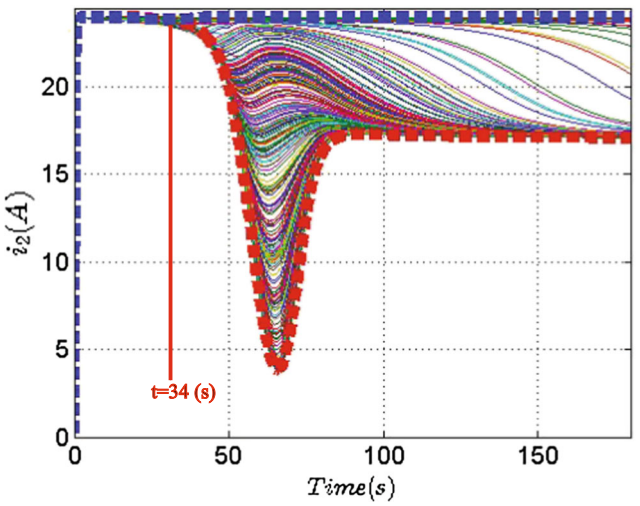

Fig. 8 The optimal (*dashed red line*) and nominal (*dashed blue line*) applied currents of the downstream set

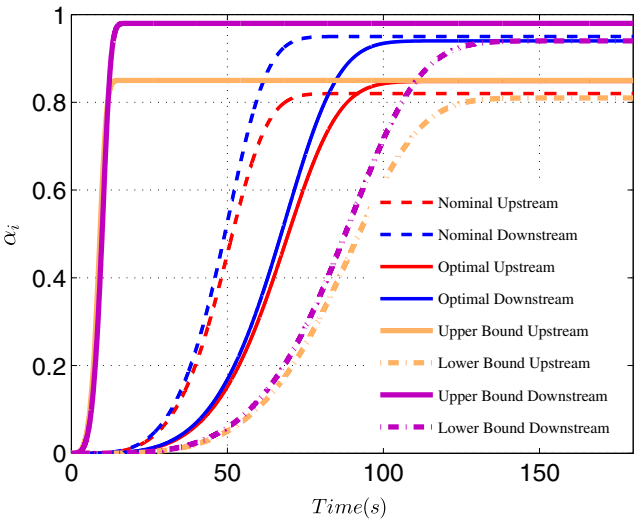

Fig. 10 The optimal and nominal valves' rotation angles including lower and upper bounds

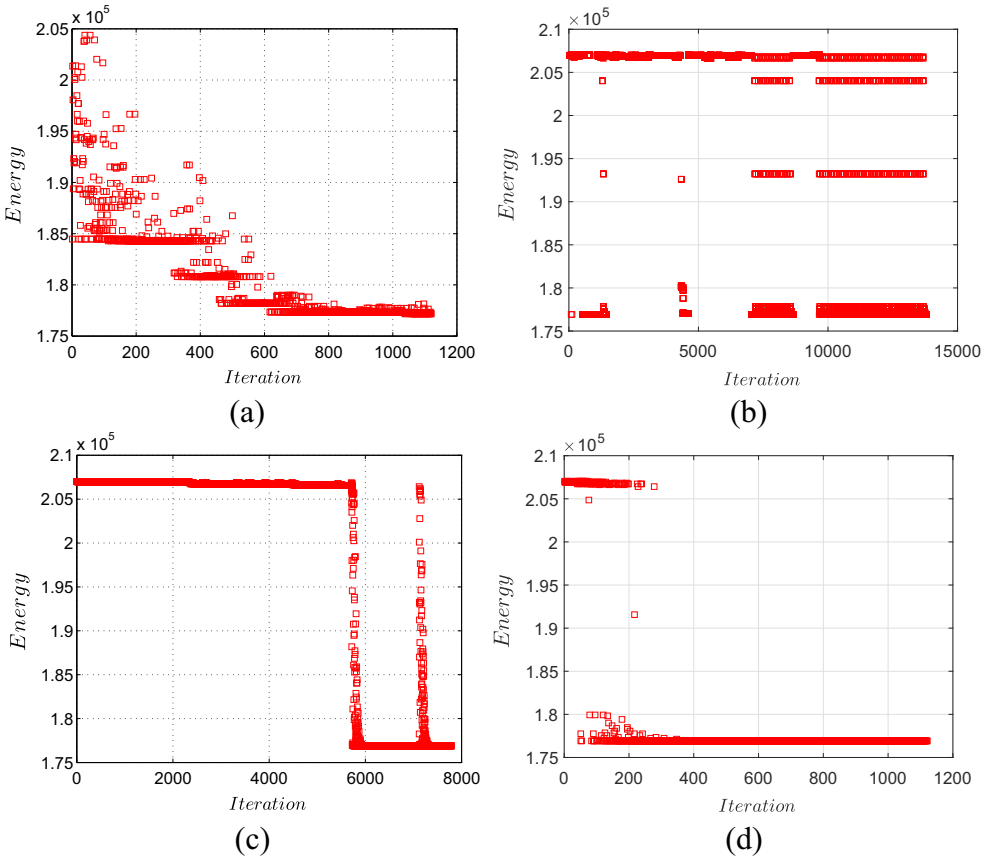

Fig. 11 The optimized lumped amount of energy: **a** GA ($E_{opm} = 177180$); **b** GB ($E_{opm} = 176900$); **c** SA ($E_{opm} = 176900$); **d** PS ($E_{opm} = 176887$)

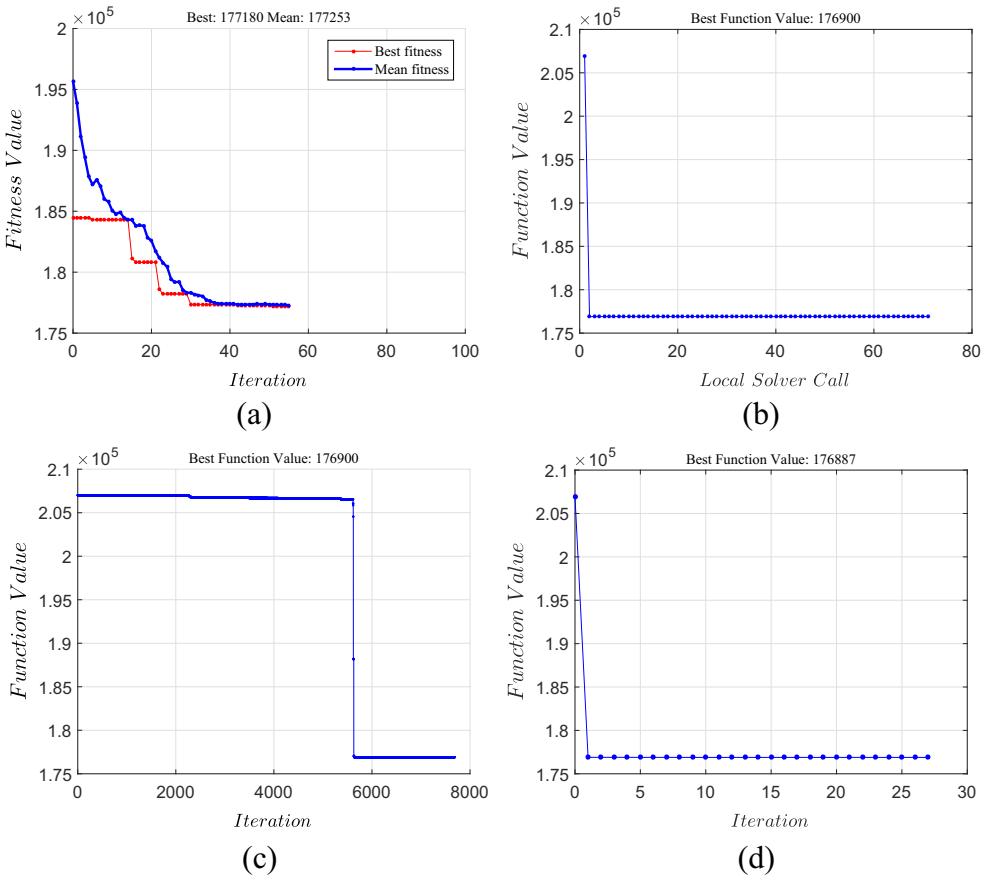

Fig. 12 The convergence history; **a** GA; **b** GB; **c** SA; **d** PS

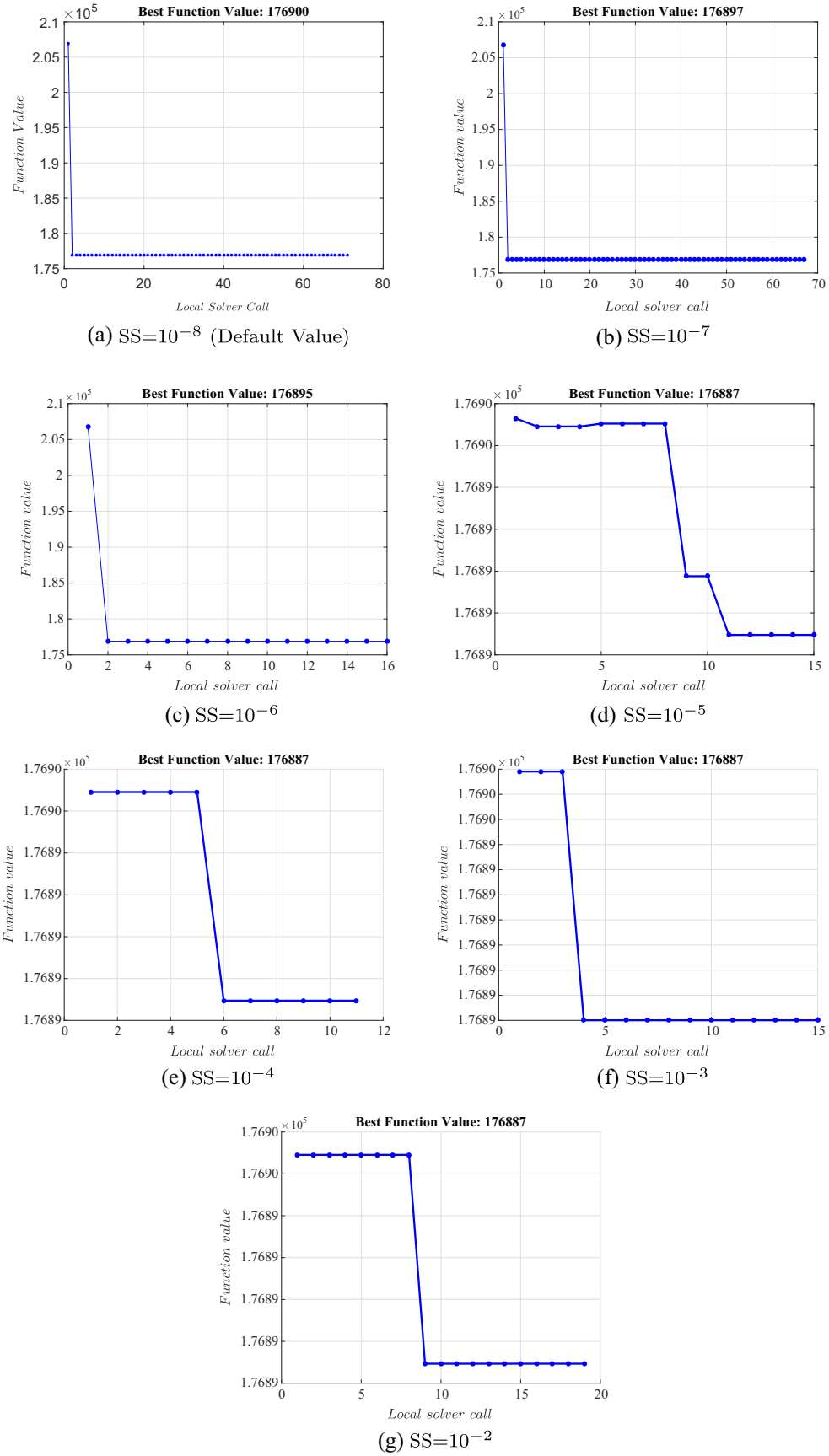

(a) SS=10^{-8} (Default Value) (b) SS=10^{-7}

(c) SS=10^{-6} (d) SS=10^{-5}

(e) SS=10^{-4} (f) SS=10^{-3}

(g) SS=10^{-2}

Fig. 13 The numerical step size (SS) analysis for the gradient based algorithm (Global Search)

the optimization effort of the gradient-based scheme shown in Figs. 5b, 6b and 11b, which we thoroughly addressed earlier, reveals the scatter-search algorithm to generate multiple starting points.

The four optimization schemes were repeatedly examined to avoid being trapped in probable local minima. The negligible difference (less than 1.5 %) among the GA, GB, SA, and PS methods would potentially indicate the global minimum value. Figure 12a–d present convergence histories of all methods revealing the monotonically decreasing cost function. Shown in Fig. 12b indicates the convergence of the cost function despite its scatter-search pattern (Fig. 11b).

Note that step size analysis (SS) is a necessary phase to be carried out in order to examine the sensitivity of the finite difference method, which has been used in the Global Search algorithm, to the amount of step size. Figure 13a–g present such a numerical analysis for a broad range of SS $= 10^{-8}$ (default value) to SS $= 10^{-2}$ evaluating its drastic effects on both the computational cost (iteration) and cost function. Note that the gradient based algorithm (13797) reveals significant gaps, with respect to the computational cost, in comparison with both the GA (1100) and PS (1170) methods. This cumbersome issue needs to be carefully addressed. To address these issues, we have to find the best value of the step size. Some useful information can be easily extracted from Fig. 13a–g, as shown in Fig. 14a and b.

Figure 14a reveals that the computational cost significantly decreases by selecting higher values of the step size. At SS $= 10^{-4}$ (circled point), the computational cost is at its minimum value (3371), which is also close to both the GA and PS ones. For the step sizes higher than 10^{-4}, the computational cost is slightly increased. From another aspect, the global minimum of the cost function is slightly lower for SS $= 10^{-4}$ (Fig. 14b) than that of the default value shown in Fig. 13a and equals, surprisingly, to the value of the PS algorithm. It is hence straightforward to conclude that the step size of SS $= 10^{-4}$ is the best one to be used in the finite difference method which we have utilized here.

Note that the computational cost of the SA algorithm shown in Fig. 11c is also considerably higher than those of both the GA and PS ones. Note that metaheuristic methods, including the GA and PS algorithms, generate a population of points at each iteration and the best point in the population then approaches an optimal solution. However, the SA algorithm generates a single point at each iteration and the sequence of points approaches an optimal solution. Therefore, the SA method has been developed to achieve global optimum by slowly converging to a final solution, making downwards move hoping to reach global optimum solution. Consequently, the computational cost (7685) of the SA algorithm looks logical with respect to both the GA and PS methods.

It is also of great interest to evaluate the effect of approach angle (θ) on the amount of energy saved. Figure 15 presents an interesting aspect of the optimization problem in that the lumped amount of energy saved for both the sets is higher for a smaller approach angle in comparison with a higher value. The physical interpretation of such an energy consumption paradigm can be found through (7) and (8). The higher approach angle yields the higher contraction resistance (R_{con}), lower P_2, and subsequently lower pressure drop across the downstream valve. Note that the downstream set has a higher share in minimizing the energy consumption by experiencing the sudden current drop (Fig. 8). The lower pressure drop of the downstream valve would result in the lower value of the helping hydrodynamic torque as previously explained via (11). The actuation unit of the downstream set located after a sharper pipe contraction (a large value of θ) has therefore less freedom to save the lumped energy than that of a smoother contraction.

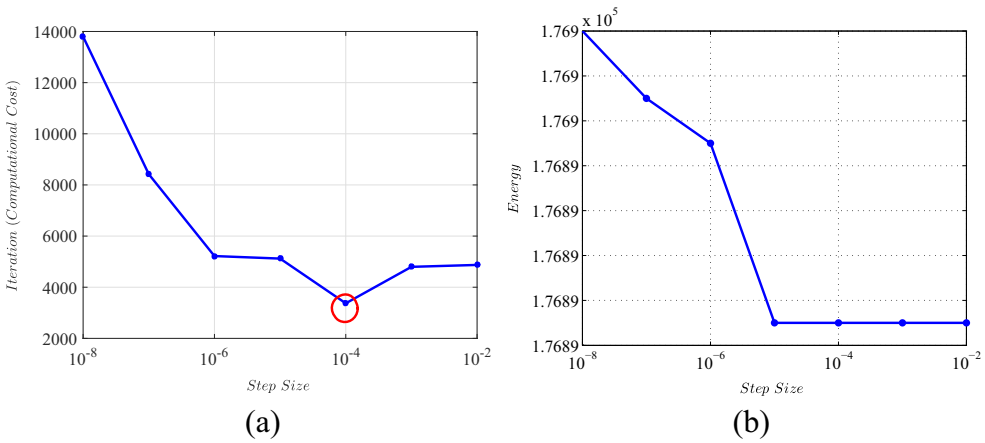

Fig. 14 The numerical step size (SS) analysis: **a** SS vs. Iteration; **b** SS vs. Energy

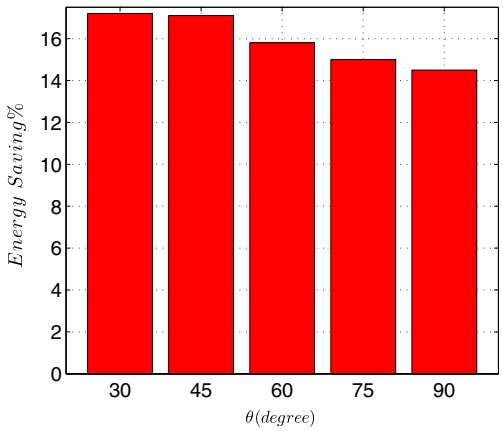

Fig. 15 The amount of saved energy vs. the approach angle

5 Conclusions and future work

In this paper, we represented a novel interconnected nonlinear model of two solenoid actuated valves subject to the different approach angles of the pipeline contraction. We revealed the significant effects of mutual interactions between the dynamics of the valves and the actuators in correlations with the flow nonlinear torques. These couplings among different elements were accurately formalized to derive a sixth order dynamic model of the whole system. We utilized particle swarm, genetic, simulated annealing, and gradient based schemes to carry out operational optimization and subsequently captured the global minimum of the lumped cost function defined as the sum of energy used in each set.

The principal results of this paper can be summarized as follows.

- The approach angle has an inverse relationship with the amount of energy saved for both the sets. The sharper pipe contraction yields the higher value of energy consumption.
- Energy can be saved by significant amounts of 17.2 %, 17 %, 16 %, 15 %, and 14.5 % for the approach angles of 30°, 45°, 60°, 75°, and 90°, respectively, with respect to nominal energies consumed in the coupled valves' motions.
- The optimal hydrodynamic torques help actuators spend a minimum level of the lumped energy.

Acknowledgments The experimental work of this research was supported by Office of Naval Research Grant (N00014/2008/1/0435). We appreciate this grant and the advice and direction provided by Mr. Anthony Seman III, the program manager.

References

Baek-Ju S, Eun-Woong L (2005) Optimal design and speed increasing method of solenoid actuator using a non-magnetic ring. In: International conference on power electronics and drives systems, pp 1140–1145

Bennett CO, Myers JE (1962) Momentum, heat, and mass transfer. McGraw-Hill, New York

Cerny V (1985) Thermodynamical approach to the traveling salesman problem: an efficient simulation algorithm. J Optim Theory Appl 45(1):41–55. doi:10.1007/BF00940812

Chakraborty I, Trawick DR, Jackson D, Mavris D (2013) Electric control surface actuator design optimization and allocation for the more electric aircraft. In: 2013 aviation technology, integration, and operations conference

Elka A, Bucher I (2009) Optimal electrode shaping for precise modal electromechanical filtering. Struct Multidiscip Optim 38(6):627–641

Grierson DE, Pak WH (1993) Optimal sizing, geometrical and topological design using a genetic algorithm. Structural Optimization 6(3):151–159

Holland HJ (1975) Adaptation in natural and artificial systems. Adaptation in Natural and Artificial Systems, Cambridge

Hughes R, Balestrini S, Kelly K, Weston N, Mavris D (2006) Modeling of an integrated reconfigurable intelligent system (IRIS) for ship design. In: Proceedings of the 2006 ASNE ship and ship systems technology (S3T) symposium

Kajima T (1995) Dynamic model of the plunger type solenoids at deenergizing state. IEEE Trans Magn 31(3):2315–2323

Karr CL, Scott DA (2003) Genetic algorithm frequency domain optimization of an anti-resonant electromechanical controller. Lecture Notes in Computer Science

Kelley CT (1999) Iterative methods for optimization. Front Appl Math 18

Kennedy J, Eberhart R (1995) Particle swarm optimization. In: Proceedings of IEEE international conference on neural networks, pp 1942–1948

Kirkpatrick S, Gelatt CD, Vecchi MP (1983) Optimization by simulated annealing. Science 220(4598):671–680. doi:10.1126/science.220.4598.671

Klimovich VI (1997) On the optimal design of the form of hydroturbine impeller blades. Struct Multidiscip Optim 13(1):29–35

Lee K, Ortiz JL, Mohtadi MA, Park YM (1988) Optimal operation of large-scale power systems. IEEE Trans Power Syst 3(2):413–420

Lequesne B, Henry R, Kamal M (1998) Magnavalve: a new solenoid configuration based on a spring-mass oscillatory system for engine valve actuation. GM Research Report E3-89

Leutwyler Z, Dalton C (2008) A CFD study of the flow field, resultant force, and aerodynamic torque on a symmetric disk butterfly valve in a compressible fluid. J Press Vessel Technol 130(2):021302

Mahdi SA (2014) Optimization of pid controller parameters based on genetic algorithm for non-linear electromechanical actuator. Int J Comput Appl 94:11–20

Massey BS, Ward-Smith J (1998) Mechanics of fluids, 7th edn. Taylor & Francis, London and New York

Messine F, Nogarede B, Lagouanelle JL (1998) Optimal design of electromechanical actuators: a new method based on global optimization. IEEE Trans Magn 34(1):299–308

Mezyk A (1994) Minimization of transient forces in an electromechanical system. Struct Multidiscip Optim 8(4):251–256

Naseradinmousavi P (2012) Nonlinear modeling, dynamic analysis, and optimal design and operation of electromechanical valve systems. PhD thesis, Villanova University

Naseradinmousavi P (2015) A novel nonlinear modeling and dynamic analysis of solenoid actuated butterfly valves coupled in series. ASME J Dyn Syst Meas Control 137(1):014505

Naseradinmousavi P, Nataraj C (2011a) A chaotic blue sky catastrophe of butterfly valves driven by solenoid actuators. In: Proceedings of the ASME 2011 international mechanical engineering congress & exposition, IMECE2011/62608

Naseradinmousavi P, Nataraj C (2011b) Nonlinear mathematical modeling of butterfly valves driven by solenoid actuators. J Appl Math Model 35(5):2324–2335

Naseradinmousavi P, Nataraj C (2012) Transient chaos and crisis phenomena in butterfly valves driven by solenoid actuators. Commun Nonlinear Sci Numer Simul 17(11):4336–4345

Naseradinmousavi P, Nataraj C (2013) Optimal design of solenoid actuators driving butterfly valves. ASME J Mech Des 135(9):094501

Naseradinmousavi P, Nataraj C (2015) Design optimization of solenoid actuated butterfly valves dynamically coupled in series. In: Proceedings of the ASME 2015 dynamic systems and control conference, vol 2: diagnostics and detection; drilling; dynamics and control of wind energy systems; energy harvesting; estimation and identification; flexible and smart structure control; fuels cells/energy storage; human robot interaction; hvac building energy management; industrial applications; intelligent transportation systems; manufacturing; mechatronics; modelling and validation; motion and vibration control applications, p V002T33A001

Naseradinmousavi P, Krstic M, Nataraj C (2016) Design optimization of dynamically coupled actuated butterfly valves subject to a sudden contraction. ASME J Mech Des 138(4):041402

Nowak L (2010) Optimization of the electromechanical systems on the basis of coupled field-circuit approach. Int J Comput Math Electr Electron Eng 20(1):39–52

Park JY, Chung MK (2006) Study on hydrodynamic torque of a butterfly valve. J Fluids Eng 128(1):190–195

Raulli M, Maute K (2005) Topology optimization of electrostatically actuated microsystems. Struct Multidiscip Optim 30(5):342–359

Sefkat G (2009) The design optimization of the electromechanical actuator. Struct Multidiscip Optim 37(6):635–644

Shi Y, Eberhart RC (1998) A modified particle swarm optimizer. In: Proceedings of IEEE international conference on evolutionary computation, pp 69–73

Sung BJ, Lee EW, Kim HE (2002) Development of design program for on and off type solenoid actuator. In: Proceedings of the KIEE summer annual conference, vol B, pp 929–931

Yu H, Li G, Zhu F, Gui Q, Li R (2007) Research on optimal operation in large-scale steam piping system. Springer Berlin Heidelberg, Hangzhou and New York, chap Challenges of Power Engineering and Environment, pp 593–596